


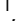









Variations in triple oxygen isotope of speleothems from the Asian monsoon region reveal moisture sources over the past 300 years

Lijuan Sha¹, Jasper A. Wassenburg^{2,3}, Lifan Sha⁴, Youwei Li¹, Shilun Zhou⁵, Qisheng Liang⁶, Jingyao Zhao¹, Jiaoyang Ruan^{2,3}, Hanying Li¹, Xinnan Zhao⁷, Pengzhen Duan⁸, Jian Wang¹, Jiayu Lu⁹, Haiwei Zhang¹, Gayatri Kathayat¹, Sasadhar Mahata¹, Fengmei Ban¹⁰, Ting-Yong Li⁶ & Hai Cheng^{1,11}

Characterization of moisture origins is crucial to understanding hydroclimatic processes. Nevertheless, documenting past atmospheric moisture contents and their sources remains challenging partially due to insufficient moisture-tracing proxies. Here, we present triple oxygen isotope compositions in 21 cave speleothems from monsoonal Asia to examine spatial moisture origin differences in eastern Asia over the past 300 years. Our data suggest an isotopic equilibrium fractionation during speleothem formation, and thus parent water ^{17}O anomalies ($\Delta^{17}\text{O}$) values reconstructed from speleothems preserve information on moisture origins and recycling across space. Notably, speleothem $\Delta^{17}\text{O}$ records exhibit a distinct geographical distribution, with low values in central-eastern and southern China, high values in northwestern and northern China, and relatively high values in the Yangtze River region. This spatial pattern underscores the diverse influence of different moisture sources regulated by regional hydrological circulation, and demonstrates the potential use of speleothem $\Delta^{17}\text{O}$ in reconstructing the moisture cycle at spatial scales.

¹Institute of Global Environmental Change, Xi'an Jiaotong University, Xi'an, China. ²Center for Climate Physics, Institute for Basic Science, Busan, Republic of Korea. ³Pusan National University, Busan, Republic of Korea. ⁴Information Centre, Department of Natural Resources of Zhejiang Province, Hangzhou, China. ⁵College of Oceanography and Space Informatics, China University of Petroleum, Qingdao, China. ⁶Yunnan Key Laboratory of Plateau Geographical Processes & Environmental Changes, Faculty of Geography, Yunnan Normal University, Kunming, China. ⁷School of Geography and Tourism, Huizhou University, Huizhou, Guangdong, China. ⁸Research Institute of Petroleum Exploration and Development, PetroChina, Beijing, China. ⁹Jiangsu Coastal Development Research Institute, Yancheng Teachers University, Yancheng, China. ¹⁰College of Resources and Environment, Shanxi University of Finance and Economics, Taiyuan, China. ¹¹State Key Laboratory of Loess and Quaternary Geology, Institute of Earth Environment, Chinese Academy of Sciences, Xi'an, China. ✉email: shalijuan@xjtu.edu.cn; cheng021@xjtu.edu.cn

Global warming has intensified ocean-to-land hydrological variability, resulting in extreme events such as floods and droughts^{1,2}, significantly affecting human life and economic development in the Asian monsoon region and elsewhere^{3,4}. Identifying the apportionment of moisture contributions from different sources is essential for understanding hydroclimate variability. However, the long-term dynamic processes determining continental-scale changes in atmospheric moisture and its sources are poorly constrained because of the absence of an appropriate proxy for effectively monitoring moisture origin and recycling on various timescales.

Recent studies reveal that distributions of triple oxygen isotope (^{16}O , ^{17}O , and ^{18}O) in various types of water (including precipitation, plants, rivers, and ponds)^{5–10}, as well as in carbonate records^{11–14}, have significantly enriched paleoclimate interpretations beyond what was possible with traditional $\delta^{18}\text{O}$ data alone. This advancement is achieved through a combination of traditional $\delta^{18}\text{O}$ data and the additional information provided by the isotope tracer $\Delta^{17}\text{O}$ ($\Delta^{17}\text{O} = \delta^{17}\text{O} - 0.528 \times \delta^{18}\text{O}$; see “Methods” section). This approach is similar to the more detailed inquiries enabled by the combination of δD and $\delta^{18}\text{O}$, as indicated by the d-excess parameter ($\text{d-excess} = \delta\text{D} - 8 \times \delta^{18}\text{O}$)^{15,16}, rather than relying on a single isotope system. As the initial step in the large-scale hydrological cycle, the $\Delta^{17}\text{O}$ values of oceanic evaporation fluxes commonly depend on relative humidity, boundary-layer aerodynamics, and isotopic gradients at the evaporation site, reflecting the similar moisture source condition on short timescales^{5,17}. Additionally, modern meteoric water studies show that additional processes, such as condensation, mixing of moisture sources, supersaturation, and terrestrial hydroclimate variations (such as moisture recycling and re-evaporation of precipitation), may also contribute to some extent to the changes in the $\Delta^{17}\text{O}$ values^{6,8,9,18–20}. In comparison to the d-excess, $\Delta^{17}\text{O}$ is less dependent on the temperature at evaporation and condensation sites^{8,18,19,21}, while the precipitation $\Delta^{17}\text{O}$ displays a relatively higher sensitivity than d-excess to terrestrial evaporation-dominated moisture recycling and re-evaporation during light rainfall events^{18,19}. Thus, the use of $\Delta^{17}\text{O}$ in combination with $\delta^{18}\text{O}$ presents a potential strategy to decipher the various fractionation processes at the remote moisture source (oceanic evaporation), en route (Rayleigh distillation, vapor mixing, and continental moisture recycling), and at the moisture sink (raindrop re-evaporation/equilibration and supersaturation of snow)^{8,9,18,19}.

Speleothem records are valuable as geological archives that have been widely used to reconstruct past climate history, mainly because of their advantages in their precise age control, geographic coverage, and high temporal resolutions²². In particular, studies of the oxygen isotope composition ($\delta^{18}\text{O}$) of speleothems have provided critical information on the evolution of Asian monsoon circulations on a wide range of timescales²³. In general, speleothem $\delta^{18}\text{O}$ values in the Asian monsoon region inherit primarily the $\delta^{18}\text{O}$ signal of precipitation²², which reflects the summer monsoon intensity or the spatial scale of the summer monsoon circulations associated with changes in moisture source and transport trajectory. However, a large number of factors can also affect the precipitation $\delta^{18}\text{O}$ and in turn speleothem $\delta^{18}\text{O}$, such as temperature, atmospheric circulation, moisture source and transport trajectory, precipitation amount, evaporation, etc.^{24,25}. Moreover, the speleothem $\delta^{18}\text{O}$, in principle, is incapable of distinguishing among water vapor sources that contribute to precipitation at the cave site. Recently, the $\Delta^{17}\text{O}$ has been applied to speleothem research^{13,14}. The $\Delta^{17}\text{O}$ integrates the effect of evaporation of water vapor at the source regions and moisture transportation that is ultimately reflected in precipitation at the cave sites²⁶. Therefore, the high-precision $\Delta^{17}\text{O}$ data derived from speleothems have the potential

to enhance our comprehension of hydroclimatic processes, particularly with respect to varying moisture sources, and to furnish additional insights that can refine the interpretation of speleothem $\delta^{18}\text{O}$ ^{13,14}.

In this study, we investigate variations of triple oxygen isotope compositions in a set of speleothems from the Asian monsoon region over the past 300 years, characterize their spatial variations, and then provide an interpretation of the mechanisms underlying the spatial pattern of $\Delta^{17}\text{O}$. Our results illuminate variations in the water vapor cycle, large-scale atmospheric circulation, and moisture sources in the Asian monsoon region.

Materials and climatology

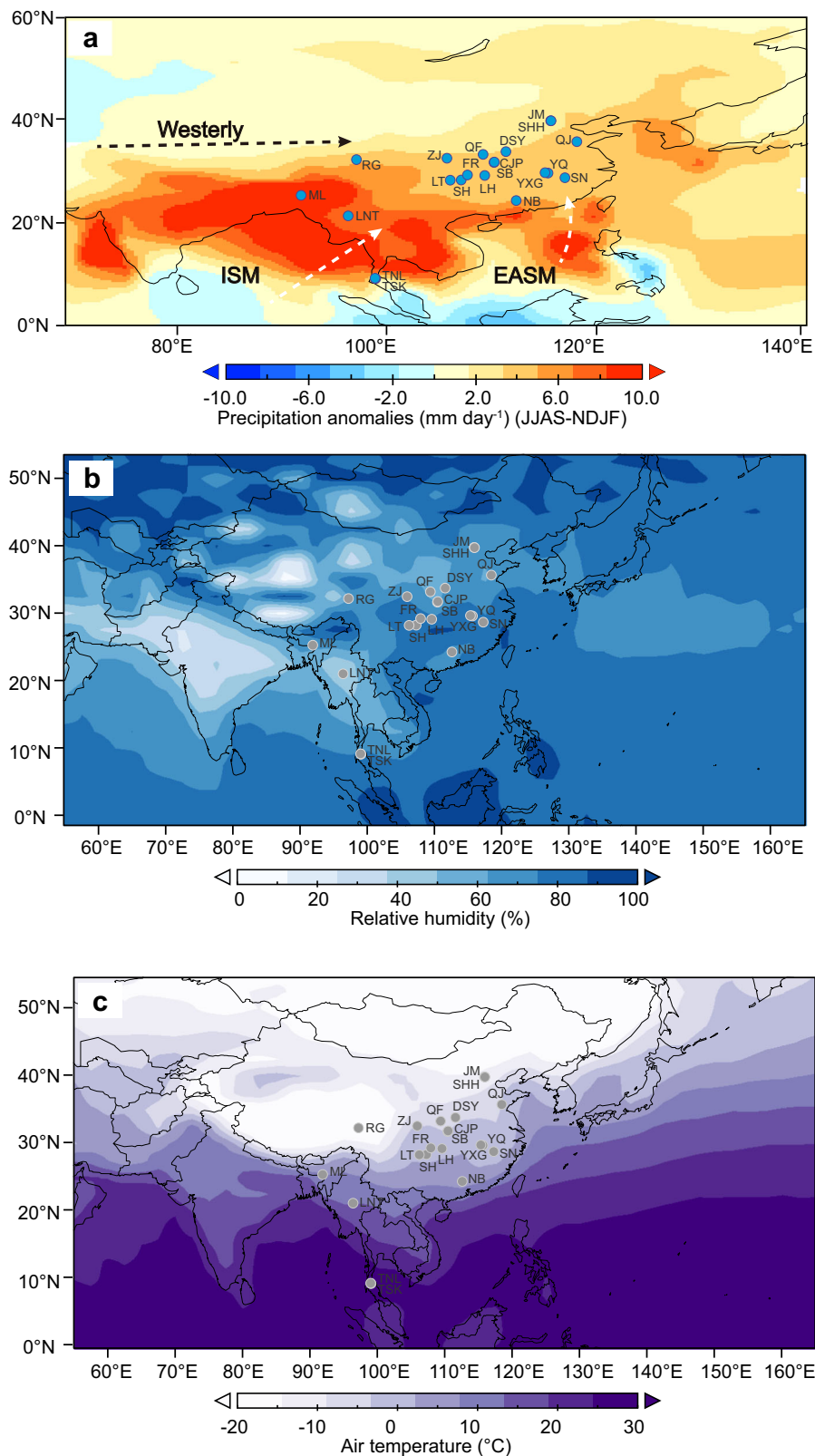
We analyzed 31 speleothem carbonate samples (Supplementary Fig. 1) collected from 21 caves across the Asian monsoon region (Supplementary Fig. 2). Most cave sites are located in central China, with fewer in northwestern and southeastern China, northeastern India, and the Indo-China Peninsula (Fig. 1). The information on the samples, including longitude-latitude and formation ages, is given in Supplementary Table 1.

The modern annual rainfall in China generally decreases from south to north, and northwestern China has the lowest annual rainfall due to its inland location remote to the ocean (Fig. 1a). Four major trajectories of moisture transport are essential to the hydroclimate across the Asian monsoon region in the Asian continent (the percentage amount of rainfall through all of the monsoonal subsystems is shown in Supplementary Fig. 3): the Bay of Bengal, the western Pacific Ocean, the Atlantic Ocean, and the northern Eurasian continent. During the summer (June to September), two subsystems of the Asian summer monsoon, the Indian summer monsoon and the East Asian summer monsoon, transport moisture from the Indian and West Pacific oceans into the Asian inland, delivering abundant rainfall^{27,28}. In contrast, the winter monsoon started from the interior of the Eurasian continent prevails in China in winter, which is associated with merely a small amount of water vapor and hence less precipitation²⁹. Additionally, the westerly influence occurs in northwestern China (such as in the northern Xingjiang region).

On the other hand, the West Pacific Subtropical High (WPSH) is also a critical system affecting the precipitation in eastern Asia. Changes in the position, shape, and strength of the WPSH³⁰ largely dominate the interannual variability of the large-scale quasi-stationary East Asian summer monsoon frontal zones. The related seasonal cycle is as follows: (1) In early May, the onset of the summer rainfall season occurs in South China, namely the pre-Meiyu season. (2) In the middle of June, the ridgeline of the WPSH moves from $\sim 15\text{--}20^\circ\text{N}$ to $\sim 20\text{--}25^\circ\text{N}$, and the rain belt shifts from South China to the Yangtze-Huaihe River Basin. This process is associated with the end of the rainy season (the first flood season) in South China and the beginning of the rainy season in the Yangtze-Huaihe River Basin. (3) In mid-July, the ridgeline reaches $\sim 25\text{--}30^\circ\text{N}$, and monsoon-associated rainfall increases over northern China. (4) In late July or early August, the subtropical high reaches the northernmost position ($\sim 30^\circ\text{N}$), the rainy season in North China begins, and the Yangtze River-Huaihe River Basin becomes dry. (5) Around the beginning of September, the ridgeline retreats southward to $\sim 25^\circ\text{N}$ and then to $\sim 20^\circ\text{N}$ at the beginning of October, and the Asian summer monsoon is close to ending.

Results and discussion

$\Delta^{17}\text{O}$ variations of speleothem carbonates and the reconstructed parent water. Our speleothem carbonates have much higher $\delta^{18}\text{O}$ values (27.132 to 36.489‰; VSMOW-SLAP) and lower $\Delta^{17}\text{O}$ values (−79 to −56 per meg; VSMOW-SLAP; see “Methods” section; Fig. 2 and Supplementary Table 2) compared to



the meteoric waters (~ 0 to -20 ‰ and -30 to 60 per meg, respectively; Fig. 2). The speleothem carbonates consist of calcite and aragonite (Supplementary Table 1), with their $\Delta^{17}\text{O}$ values at the formation, exhibiting no notable variation³¹. Upon graphing speleothem $\Delta^{17}\text{O}$ against $\delta^{18}\text{O}$, we observe slopes of -1.018 per meg/‰ for all samples (Fig. 3a) and -0.996 per meg/‰ excluding the result from the Rige Cave located in the high-altitude region

(Fig. 3c). Moreover, the speleothems $\delta^{17}\text{O}$ versus $\delta^{18}\text{O}$ plots show a slope of 0.527 (Fig. 3b, d). These values fall within the near-horizontal trend defined by the range of -1 to 0 per meg/‰ for the carbonate $\Delta^{17}\text{O}$ versus $\delta^{18}\text{O}$ space, and $\delta^{17}\text{O}$ versus $\delta^{18}\text{O}$ slopes of 0.527 – 0.528 , bolstering the interpretations linked to climate determinants rather than ‘cave kinetic process’ (e.g., fast degassing at the drip site and prior calcite precipitation) in this

Fig. 1 Map of cave locations, precipitation, surface relative humidity (%), and air temperature (°C). **a** The precipitation amount is expressed as the difference between June through September (JJAS) and November through February (NDJF) from 1980 to 2010 in the western Pacific and East Asia, based on the data from the Global Precipitation Climatology Project (GPCP)⁷⁵. **b** Annual surface relative humidity (1980–2010) and **(c)** annual air temperature (1991–2020) are based on the data from National Centers for Environmental Prediction/National Center for Atmospheric Research, NCEP/NCAR (<https://www.esrl.noaa.gov>)⁷⁶. The site locations of the speleothem samples are in the Asian monsoon region (cave information are listed in Supplementary Table 1). Blue and gray circles show cave sites: NB-Niubi Cave (112.58°E, 24.26°N, 174 m a.s.l.)⁷⁷, SN-Shennong Cave (117.25°E, 28.70°N, 383 m a.s.l.)⁷⁸, YQ-Yongquan Cave (115.65°E, 29.61°N, 100 m a.s.l.), SH-Shuanghe Cave (107.28°E, 28.25°N, 1170 m a.s.l.), LT-Longtan Cave (106.22°E, 28.22°N, 1230 m a.s.l.), FR-Furong Cave (107.90°E, 29.22°N, 480 m a.s.l.)⁷⁹, LH-Lianhuan Cave (109.55°E, 29.15°N, 455 m a.s.l.)⁸⁰, SB-Sanbao Cave (110.43°E, 31.67°N, 1900 m a.s.l.)²³, YXG-Yangxingui Cave (115.35°E, 29.68°N, 400 m a.s.l.), CJP-Cijiaping Cave (110.47°E, 31.76°N, 2000 m a.s.l.), QJ-Qujia Cave (118.42°E, 35.71°N, 456 m a.s.l.)⁸¹, ZJ-Zhangjia Cave (105.92°E, 32.51°N, 680 m a.s.l.), QF-Qianfo Cave (109.38°E, 33.23°N, 1500 m a.s.l.), DSY-Dongshiya Cave (111.57°E, 33.77°N, 840 m a.s.l.)⁸², JM-Jimao Cave (115.88°E, 39.81°N, 330 m a.s.l.), SHH-Shihua Cave (115.93°E, 39.78°N, 251 m a.s.l.)⁸³, RG-Rige Cave (97.20°E, 32.22°N, 4252 m a.s.l.)⁸⁴, TNL-Tham Nhong-Lha Cave (99.00°E, 9.10°N, 112 m a.s.l.), TSK-Tham Sing Khon Cave (99.04°E, 9.04°N, 106 m a.s.l.), LNT-Lin Noe Twin Cave (96.41°E, 21.24°N, 1220 m a.s.l.), ML-Mawmluh Cave (91.88°E, 25.26°N, 1160 m a.s.l.). The abbreviation of a.s.l. indicates above sea level. Dashed arrows depict wind directions of the Indian summer monsoon (ISM; white), East Asian summer monsoon (EASM; white), and the mid-latitude westerly (black).

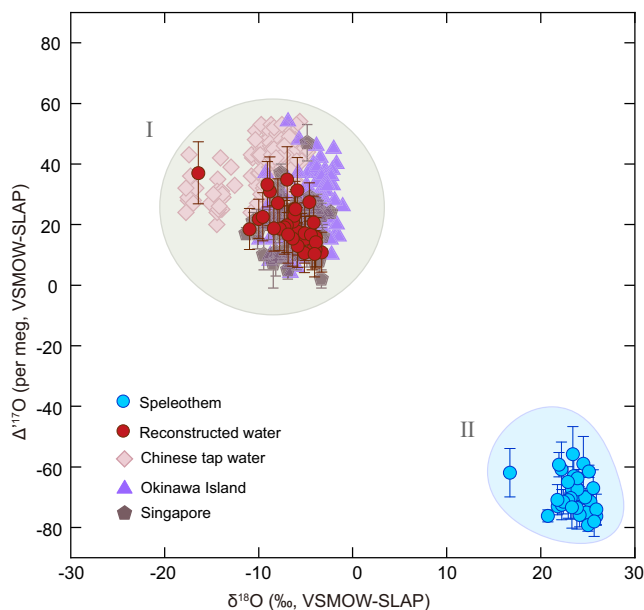


Fig. 2 Plots of $\delta^{18}\text{O}$ versus $\Delta^{17}\text{O}$ for water and carbonate samples. Group I is meteoric water in the Asian monsoon region and parent water of speleothem carbonates. Group II is speleothem carbonates. As expected, the calculated $\delta^{18}\text{O}$ – $\Delta^{17}\text{O}$ values of the parent water of speleothems (Group I) are similar to the meteoric water^{9,17,37}. All data are in VSMOW–SLAP, and the $\Delta^{17}\text{O}$ values of speleothem samples are normalized to Wostbrock et al.⁶¹. The error is based on the standard deviation (1σ SD) for each sample.

hydrological stage¹³. Additionally, the relative humidity is close to 100% in most of the study caves, rendering evaporation within the caves insignificant. As a result, these observations suggest that the carbonate deposition processes in the caves are virtually under the isotope equilibrium without noticeable effect of the ‘kinetic isotope fractionation’^{13,24,32,33}.

The growth of authigenic minerals entails mass fractionation laws of precipitation reactions, variations in the $\Delta^{17}\text{O}$ of the waters from which sedimentary minerals precipitate, and equilibrium exchanges after initial authigenic formation^{31,34}. Based on the cave monitoring results from Furong Cave (southwestern China; Fig. 1), the $\Delta^{17}\text{O}$ values of the cave dripwater inherit the $\Delta^{17}\text{O}$ signals of precipitation at the cave site (Supplementary Table 3). The parent water $\Delta^{17}\text{O}$ reconstructed from speleothem carbonates closely resembles the cave dripwater within uncertainties (Supplementary Table 3). Therefore, the contemporary speleothem $\Delta^{17}\text{O}$ values essentially reflect the

precipitation $\Delta^{17}\text{O}$ signal, thus serving as an indicator of the conditions under which carbonate precipitates^{31,35}.

The reconstructed parent water from speleothem carbonates (see ‘Methods’ section) has $\delta^{18}\text{O}$ values ranging from -16.406 to -3.920 ‰, and the $\Delta^{17}\text{O}$ values from 11 to 37 per meg (Fig. 2). The average of the reconstructed parent water $\Delta^{17}\text{O}$ values is 20 ± 7 per meg, which is comparable to the average value of 22 ± 11 per meg for the precipitation in the subtropical regions (VSMOW–SLAP; Fig. 2)^{6,9,17}. On the continental scale, the mean reconstructed $\Delta^{17}\text{O}$ values of the parent waters are 32 ± 4 , 21 ± 6 , and 15 ± 3 per meg in northern China, central China, and the southern Asian monsoon region (Fig. 4), respectively. Thus, the regional differences in precipitation oxygen isotopes in the Asian monsoon region are likely related to their different water vapor sources and other processes (such as condensation, continental recycling, and sub-cloud re-evaporation)^{8,9,18,19}.

The $\delta^{18}\text{O}$ – $\delta^{17}\text{O}$ slopes of the local meteoric water line for the reconstructed parent water from three regions (northern and north-western China, central China, and the southern Asian monsoon region) are between 0.524 and 0.526 (Supplementary Fig. 4), with the lowest slope of 0.524 in northern and northwestern China (Supplementary Fig. 4a). Our calculated triple oxygen isotope values for speleothem parent waters fall along a line with the slope of 0.525 (± 0.0010 , 1σ SD) in a cross plot of $\delta^{17}\text{O}$ versus $\delta^{18}\text{O}$ (Supplementary Fig. 4d), which is smaller than the 0.528 slope of the global meteoric water line^{5,8,36}. The slopes for water vapor equilibrium fractionation and diffusion fractionation are 0.529 and 0.518, respectively⁵. Importantly, the Rayleigh distillation slope ($\lambda_{\text{Rayleigh}} = 0.528$) closely aligns with the global meteoric water line⁸. In principle, the sub-cloud re-evaporation processes during precipitation affect the raindrops from small rainfall events, leading to strong isotopic dynamic fractionation^{8,19} and consequently a smaller slope and intercept for the local meteoric water line. However, the available triple oxygen isotope data do not fit a single global meteoric water line⁸. For example, the slope of the local meteoric water line in the tropical region of Singapore, Okinawa in subtropical Japan, and the Arctic are 0.528³⁷, 0.5296¹⁷, and 0.5299³⁸, respectively. Such disparities may stem from variations in water type, sampling bias due to high concentration of samples in small regions, or insufficient data⁸. Accordingly, the relationship between $\delta^{18}\text{O}$ and $\delta^{17}\text{O}$ investigated in this study may capture information pertinent to Rayleigh and/or equilibrium fractionation processes and factors such as moisture source, transport path, and climatic condition changes.

Continental-scale variations in triple oxygen isotope in the Asian monsoon region. The $\Delta^{17}\text{O}$ records from speleothem carbonates and reconstructed parent water exhibit no apparent

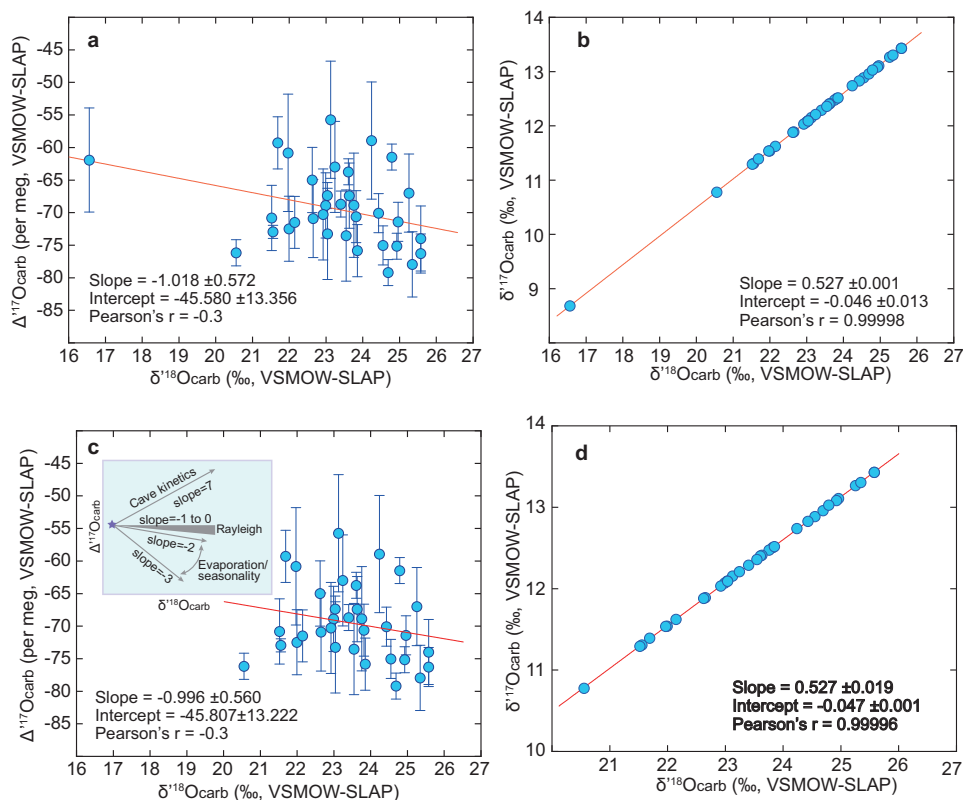


Fig. 3 Plots of $\delta^{17}\text{O}$ and $\Delta^{17}\text{O}$ versus $\delta^{18}\text{O}$ of speleothem carbonates. The $\Delta^{17}\text{O}$ versus $\delta^{18}\text{O}$ (a) and $\delta^{17}\text{O}$ versus $\delta^{18}\text{O}$ (b) space and calculated trends for the data from all the speleothem samples, respectively. The $\Delta^{17}\text{O}$ versus $\delta^{18}\text{O}$ (c) and $\delta^{17}\text{O}$ versus $\delta^{18}\text{O}$ (d) space and calculated trends for the data without the result from Rige cave in the high-altitude area (Qinghai province in northern China), respectively. The insert figure in (c) shows the summary of triple oxygen isotope drivers relevant to speleothem triple oxygen isotopes in $\Delta^{17}\text{O}$ versus $\delta^{18}\text{O}$ space¹³. The red line is the regression line of the speleothem dataset. $\delta^{17}\text{O} = 1000 \times \ln(1 + \Delta^{17}\text{O}/1000)$ and $\delta^{18}\text{O} = 1000 \times \ln(1 + \delta^{18}\text{O}/1000)$. The error bars show the measurement uncertainty. The error is based on the standard deviation (1σ SD) for each sample.

correlations with continental-scale precipitation amount anomalies (Fig. 1a), annual relative humidity (Fig. 1b), temperature (Fig. 1c), or altitude (Supplementary Fig. 2b) in the Asian monsoon region. Similarly, the continental-scale precipitation $\delta^{18}\text{O}$ shows the common pattern that the maximum precipitation $\delta^{18}\text{O}$ values generally occurred in winter (from November to February) and gradually decreased to reach their minimum during summer (from June to September) (Supplementary Fig. 5). Influencing factors such as water vapor transport distance and the Rayleigh distillation effect during the water vapor transport process can influence the levels and characteristics of $\delta^{18}\text{O}$ in modern climatology^{16,39,40}, leading to the minimum $\delta^{18}\text{O}$ values during the strong summer monsoon seasons (Supplementary Fig. 5). Therefore, we suggest that large-scale processes—such as atmospheric conditions at the moisture source, along moisture transport trajectories, and moisture source changes—have a greater impact on the continental-scale speleothem $\Delta^{17}\text{O}$ values than local climatic (local precipitation amount, relative humidity, and temperature) and geographical conditions. Nevertheless, further studies are needed to characterize to what extent these factors can affect the observed $\Delta^{17}\text{O}$ values inferred from speleothem data.

The spatial interpolation (see “Methods” section) of the speleothem carbonates $\Delta^{17}\text{O}$ at the national scale in Asian monsoon region shows a ‘quadrupole’ pattern with low $\Delta^{17}\text{O}$ values in coastal regions (e.g., Thailand and Guangdong province in southern China) and most Chinese inland cave sites (Fig. 4). This pattern diverges from Chinese tap water results⁹, which do not display a clear pattern, likely due to the complex interplay between non-local water and local precipitation isotopic signals⁹,

despite tap water being a useful initial reference for understanding the continental-scale $\Delta^{17}\text{O}$ variation in these regions.

Generally, the annual rainfall and relative humidity of study sites along the coastal regions remain relatively high throughout the year (Fig. 1b), leading to saturated or supersaturated atmospheric water vapor content and diminishing secondary evaporation under the clouds during raindrop descent. Given their proximity to oceanic moisture sources and their relatively short moisture trajectories, the speleothem and parent water $\Delta^{17}\text{O}$ values from coastal regions serve as direct proxies for the conditions of moisture sources. Furthermore, the speleothem and parent water $\Delta^{17}\text{O}$ values from most Chinese inland cave sites exhibit a near-horizontal trend, reflecting the aforementioned Rayleigh distillation processes. Therefore, the low speleothem $\Delta^{17}\text{O}$ values from most Chinese inland cave sites could inherit the large-scale hydroclimate processes similar to coastal regions. The 7-day air mass back-trajectories calculated using the Hybrid Single-Particle Lagrangian Integrated Trajectory model (HYSPPLIT) algorithm (see “Methods” section) show that during summer, the air masses in China are affected by both the local hydroclimatic systems and the Asian summer monsoon, including the East Asian monsoon from the West Pacific Ocean and the Indian summer monsoon from the Indian Ocean (Supplementary Fig. 3). Since the summer monsoon supplies most of the annual rainfall to the Asian monsoon region (Supplementary Figs. 3 and 5), we suggest that the observed $\Delta^{17}\text{O}$ spatial pattern in the coastal and inland regions that, to some extent, may have also been modified by initial water vapor evaporation conditions^{17,26,41}, such as the Indian and West Pacific oceans.

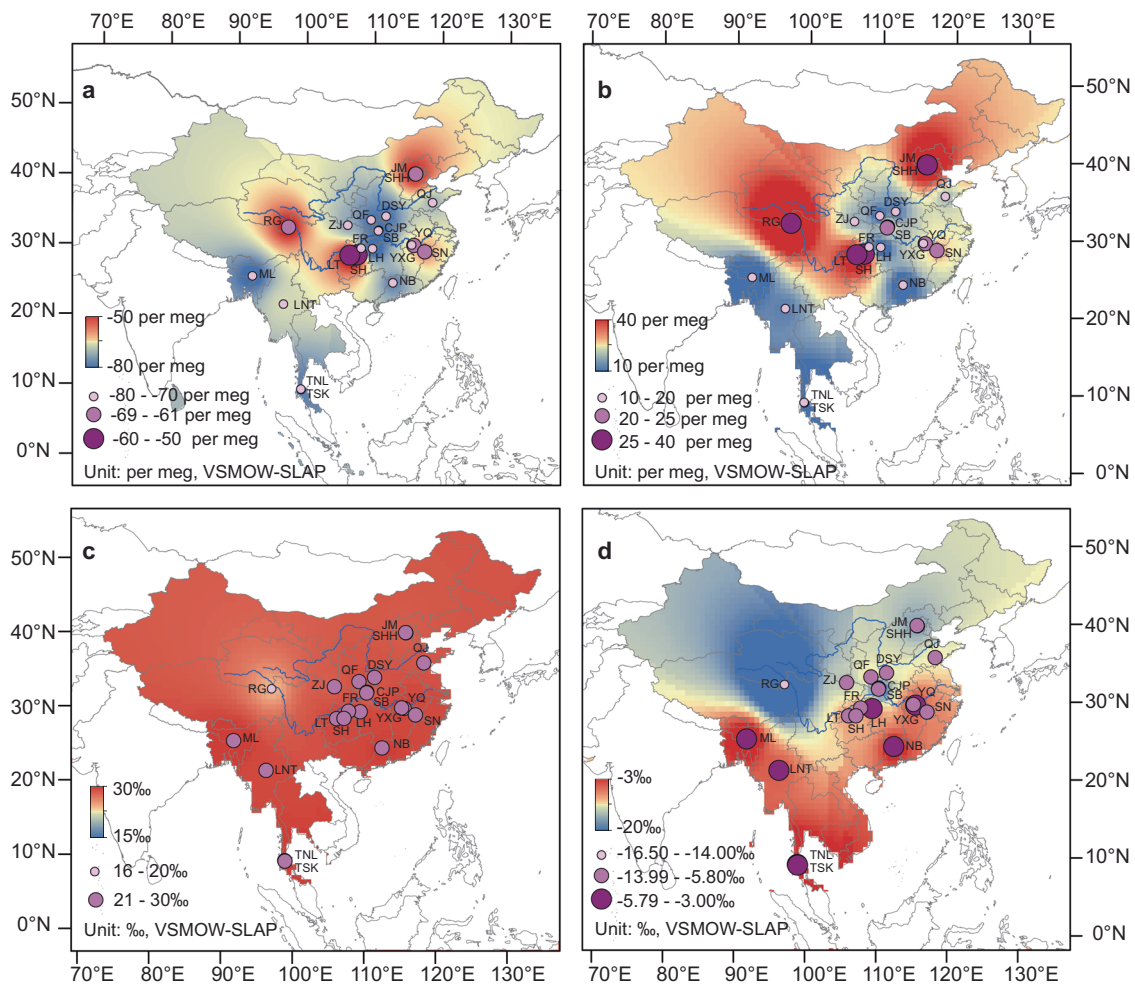


Fig. 4 Interpolated carbonates and parent waters $\delta^{18}\text{O}$ and $\Delta^{17}\text{O}$ values for speleothems from the Asian monsoon region. The interpolated maps for $\Delta^{17}\text{O}$ values of speleothems (a) and reconstructed parent water (b), respectively. The interpolated maps for $\delta^{18}\text{O}$ values of speleothems (c) and reconstructed parent water (d), respectively. Symbol size represents isotopic values. The interpolated maps of $\delta^{18}\text{O}$ and $\Delta^{17}\text{O}$ values of speleothems were generated using inverse distance weighted (IDW) interpolation⁷³. The locations of all sample sites are given in Fig. 1 and Supplementary Table 1.

Several high $\Delta^{17}\text{O}$ values occur in relatively high-latitude (Beijing) and high-altitude (Qinghai province in northwestern China) areas. The speleothem carbonate and reconstructed parent water $\Delta^{17}\text{O}$ records show no noticeable correlations with latitude and altitude on the continental scale (Supplementary Fig. 2b). In contrast, a previous study revealed a strong latitudinal effect on the tap water $\Delta^{17}\text{O}$ from -6 to 43 per meg across the USA⁶. Indeed, analyses of mid-latitude rainfall δD and $\delta^{18}\text{O}$ show that moisture recycling plays a vital role in the continental moisture balance^{42,43}. The evaporative recycling of continental moisture could contribute to the substantial local effect by increasing the $\Delta^{17}\text{O}$ in the vapor flux and inducing positive $\Delta^{17}\text{O}$ shift in the resultant mixed vapor, thus resulting in slight increases in precipitation $\Delta^{17}\text{O}$ ^{8,44}. Moreover, moisture recycling processes, such as the sublimation of surface snow, can potentially elevate precipitation $\Delta^{17}\text{O}$ and subsequently speleothem $\Delta^{17}\text{O}$ values⁴⁵. Additionally, the triple oxygen isotope compositions of speleothems formed from the dripwater follow the equilibrium line between carbonate and water¹⁴. In the context of precipitation originating from consistent moisture sources (such as the Indian and Pacific oceans), speleothems in the colder and/or higher-altitude caves in northeastern China would result in lower $\delta^{18}\text{O}$ and higher $\Delta^{17}\text{O}$ values^{14,31} compared to those in central China during the process of speleothem formation. We, therefore, suggest that the high speleothem $\Delta^{17}\text{O}$ values from high-altitude

areas are likely related to the contribution of moisture from continental recycling in relatively arid regions (e.g., northwestern China), or low cave temperature in high-altitude regions (e.g., northern China), or the moisture recycling processes.

Intriguingly, several inland cities around the Yangtze River have slightly higher speleothem and reconstructed parent water $\Delta^{17}\text{O}$ values. Our speleothem $\Delta^{17}\text{O}$ results show differences between adjacent cave sites in southwestern China (e.g., Longtan and Shuanghe caves from Guizhou province in southwestern China, and Furong cave in the vicinity of Chongqing city in southwestern China) (Fig. 1 and Supplementary Table 1), indicating different water sources or mixing water sources in these caves^{6,13}. Thus, we suppose that the higher $\Delta^{17}\text{O}$ values are likely caused by the combination of local moisture recycling effects and/or changes in moisture source. In inland cave sites, the higher values of $\Delta^{17}\text{O}$ are most likely due to the input of the recycling of water vapor.

Possible mechanisms controlling the distribution of $\Delta^{17}\text{O}$. The interpolated speleothem $\Delta^{17}\text{O}$ data presents a spatial pattern with lower values over coastal regions and most Chinese inland cave sites and higher values over northwestern and northern China (Fig. 4). Lower $\Delta^{17}\text{O}$ values in central and southern China (Fig. 4) as previously discussed, signify moisture sources originating from the Pacific and Indian oceans (Supplementary Fig. 3).

However, relatively higher $\Delta^{17}\text{O}$ values are displayed across the Yangtze River region.

HYSPLIT air mass back-trajectories results suggest that polar air masses and continental sources may contribute to the winter or pre-meyu (early May) precipitation in China (Supplementary Fig. 3). Oxygen isotope values vary in tandem with continental moisture recycling when the trajectories of polar air masses contribute moisture to winter or pre-meyu precipitation. Indeed, the $\Delta^{17}\text{O}$ values in surface snow and water vapor at NEEM (North Greenland Eemian Drilling Project; Greenland), mainly sourced from polar regions, have lower values during summer and the highest values from winter to spring, with an average value of 50 (± 11) per meg (VSMOW-SLAP)⁴⁶. Furthermore, the triple oxygen isotope records from the USA, where precipitation in high-latitude areas is usually influenced by westerly moisture, display elevated $\Delta^{17}\text{O}$ values (31 to 43 per meg)⁶. These support the suggestion that the westerly and polar air masses sources may influence precipitation and contribute to higher $\Delta^{17}\text{O}$ in some areas of China during the winter and/or pre-Meyu season. Therefore, the moisture source influences the triple oxygen isotope composition of precipitation caused by different conditions (e.g., relative humidity) at the moisture source regions and varying air mass histories when moisture uptake occurs^{47,48}.

Seasonal fluctuations in the position, shape, and intensity of the WPSH directly correlate with the distribution of rainfall in China^{49–51}. The low-level jet stream along the northwestern periphery of the WPSH transports copious amounts of water vapor to East Asia. Consequently, any alteration in the WPSH impacts the Meiyu front, affecting the convergence of tropical water vapor with extratropical airflows^{30,52}. When the WPSH strengthens and moves equatorward³⁰, the rain belt is located along the Yangtze River valley, resulting in precipitation during the pre-Meyu and Meiyu seasons, produced by the Meiyu front. The front remains relatively stationary, exemplifying the interaction between warm, moist air from the tropics and cold water vapor sources from the Arctic or local regions contributing to the precipitation^{53,54}. In the context of global warming, the anomalously cold air represents an intrusion, which enhances convergence, stimulates convection, and increases the frequency of heavy rainstorms.

Furthermore, higher $\Delta^{17}\text{O}$ values in the northern and Tibetan Plateau regions are caused by moisture from the arid north, which evidently has undergone distinct local moisture recycling. Additionally, the latitudinal position of the westerlies could affect the seasonality of the East Asian summer monsoon⁵⁵, with the seasonal migration of the westerlies from the south of the Tibetan Plateau to the north, corresponding to the transition from the pre-Meyu to the Meiyu, and the migration of the westerlies away from the northern edge of the plateau corresponds to the transition from the Meiyu to the midsummer period⁵⁶.

The changes in the Arctic not only influence temperature and precipitation in the midlatitudes but also contribute to severe convection^{54,57}. In the context of anthropogenic global warming, warm air infiltrates over anomalously cold air from the Arctic regions, enhancing convergence, stimulating convection, and increasing the frequency of rainstorms^{57,58}. Notably, the amplified warming trend in the Indian Ocean–western Pacific has prompted the westward extension of the WPSH since the late 1970s, attributable to cooling in the central and eastern tropical Pacific and augmented monsoon condensational heating in the equatorial Indian Ocean/Maritime Continent^{55,56}. Given these findings and observations of continental-scale variations in the triple oxygen isotope of speleothems from the Asian monsoon region, the interactions between Arctic teleconnections and other regional and distant feedback processes could potentially result in more persistent hot-dry extremes in the future, particularly in northern China and the Yangtze River region^{4,57}.

Conclusions

We have characterized the spatiotemporal variability of $\delta^{18}\text{O}$ and derived $\Delta^{17}\text{O}$ values of speleothem carbonates from the Asian monsoon region (21 sites) over the past 300 years and attempted to reconstruct the spatial pattern of the Asian monsoon development. The results show that $\Delta^{17}\text{O}$ variations of the speleothems varied between -78 and -56 per meg with a mean value of -70 ± 6 per meg. The reconstructed parent water $\delta^{18}\text{O}$ values ranged from -16.406‰ to -3.920‰ , and the $\Delta^{17}\text{O}$ values ranged from 11 to 37 per meg with an average of 20 ± 7 per meg.

The speleothem and reconstructed parent water $\Delta^{17}\text{O}$ values display a ‘quadrupole’ pattern, characterized by low $\Delta^{17}\text{O}$ values in coastal regions (such as Thailand and the Guangdong province in southern China) and most Chinese inland cave sites. Conversely, higher values are observed in high-altitude and north-western China due to their location deep in the continental interior and far away from the ocean, leading to more remarkable continental moisture recycling (including sublimation of surface snow) and changes in the water source. A positive $\Delta^{17}\text{O}$ anomaly is apparent in the Yangtze River valley, primarily attributable to the water vapor sources from the Arctic or local regions. Overall, the continental-scale variations in the triple oxygen isotopes of speleothems from the Asian monsoon region reveal large-scale atmospheric circulation patterns and associated complex water vapor sources.

Methods

Speleothem $\Delta^{17}\text{O}$ measurements. $\Delta^{17}\text{O}$ values of the CO_2 of the speleothem carbonate samples were precisely measured based on O_2 - CO_2 Pt-catalyzed oxygen isotope equilibrium^{14,59}. All the measurements were performed at the Institute of Global Environmental Change of Xi'an Jiaotong University (China). The major steps included: (i) extraction of CO_2 gas from carbonates using concentrated phosphoric acid at 25°C ; (ii) equilibration of the extracted CO_2 and O_2 with known isotope compositions for 30 min under Pt-catalysis at 750°C ; (iii) cryogenic separation of the two post-equilibration gases; (iv) measurement of the equilibrated O_2 using a MAT-253 Stable Isotope Ratio Mass Spectrometer, and the calculation of $\Delta^{17}\text{O}$ values. The $\delta^{18}\text{O}$ values of the CO_2 standard gases were directly measured and normalized to the concurrent analyses of standard NBS18, which were then cross-calibrated to standard IAEA603. A two-point linear normalization method⁶⁰ was used to normalize the measured $\delta^{18}\text{O}$, $\delta^{17}\text{O}$, and $\Delta^{17}\text{O}$ values, using the published high-precision values of standards NBS18 and IAEA603 presented by Wostbrock et al.⁶¹.

The measured $\delta^{18}\text{O}$ and $\Delta^{17}\text{O}$ values of CO_2 extracted from carbonates were calculated using the factors of 1.01025 ($^{18}\alpha_{\text{CO}_2/\text{carbonate}}$)⁶² and 1.00535 ($^{17}\alpha_{\text{CO}_2/\text{carbonate}}$)⁶¹ for the oxygen fractionation between CO_2 and carbonate, respectively, during the phosphoric-acid digestion process. We used an exponent of 0.523 for $\theta_{\text{CO}_2/\text{carbonate}}$ to calculate $^{17}\alpha_{\text{CO}_2/\text{carbonate}}$ during phosphoric-acid digestion at 25°C ⁶¹.

Water $\Delta^{17}\text{O}$ measurements. The $\delta^{18}\text{O}$ and $\delta^{17}\text{O}$ values of water samples were measured using Picarro-L2140i at the Xi'an Jiaotong University Isotope Laboratory, Xi'an, China. Each sample was measured at least three times. In order to avoid the memory effect associated with the continuous flow method, ten injections were conducted every time, and the first three measurements were discarded⁶³.

The results were calibrated against the VSMOW and SLAP standards by a two-point calibration, with $\delta^{18}\text{O}$ and $\delta^{17}\text{O}$ values as follows: VSMOW (0‰, 0‰) and SLAP (-55.5‰ , -29.7‰)⁶⁴.

We also employed three lab working standards with $\delta^{18}\text{O}$ and $\delta^{17}\text{O}$ values as follows: LAB1 (−1.270‰, −0.680‰), LAB2 (−11.651‰, −6.141‰) and LAB3 (−17.619‰, −9.315‰). The analytical precisions (1 σ SD) were better than ± 0.025 ‰ for $\delta^{17}\text{O}$ and $\delta^{18}\text{O}$ ⁶³. Typical in-sample $\Delta^{17}\text{O}$ precisions (1 σ SD) in water standards were 10 per meg, respectively.

^{230}Th dating method. Ages of speleothem samples were established by ^{230}Th dating. Dating was performed at the Institute of Global Environmental Change of Xi'an Jiaotong University (China), using a Neptune Plus Multi-Collector Inductively Coupled Plasma Mass Spectrometer (MC-ICP-MS). The chemical and instrumental procedures are described in Edwards et al.⁶⁵ and Cheng et al.⁶⁶.

Notations in the triple oxygen isotope system. Oxygen-isotope ratios ($^{17}\text{O}/^{16}\text{O}$ and $^{18}\text{O}/^{16}\text{O}$) are reported using the δ notation relative to the Vienna Standard Mean Ocean Water (VSMOW) or Vienna Pee Dee Belemnite (VPDB) standard:

$$\delta^{18}\text{O} = ((^{18}\text{O}/^{16}\text{O})_{\text{sample}} / (^{18}\text{O}/^{16}\text{O})_{\text{standard}} - 1) \times 1000 \quad (1)$$

and

$$\delta^{17}\text{O} = ((^{17}\text{O}/^{16}\text{O})_{\text{sample}} / (^{17}\text{O}/^{16}\text{O})_{\text{standard}} - 1) \times 1000 \quad (2)$$

The δ notation is expressed as per mil (parts per thousand, ‰).

The definition of $\Delta^{17}\text{O}$ defines the deviation of triple oxygen isotope data from a reference relationship between $\delta^{17}\text{O}$ and $\delta^{18}\text{O}$, which is expressed in the linearized form²⁶

$$\Delta^{17}\text{O} = (\delta^{17}\text{O} - 0.528 \times \delta^{18}\text{O}) \times 1000 \quad (3)$$

where, $\delta^{17}\text{O} = 1000 \times \ln(1 + \delta^{17}\text{O}/1000)$ and $\delta^{18}\text{O} = 1000 \times \ln(1 + \delta^{18}\text{O}/1000)$.

Here, 0.528 is the slope of the $\delta^{18}\text{O}$ - $\delta^{17}\text{O}$ reference line commonly used in hydrological studies⁵. A recent study suggested that triple oxygen isotope data may not always fit this global meteoric water line⁸. In addition, several studies have indicated that even the $\Delta^{17}\text{O}$ value of standard SLAP2 is non-zero ($\lambda = 0.528$)⁶¹ and meteoric waters should fall on a curvilinear trend²⁶. However, in this study, we still used 0.528 to enable comparison with the reported triple oxygen isotope data in much of the previous literature. All reported isotope data are for the gaseous phase only. The magnitude is minimal for ^{17}O anomalies; thus, we report this value in 'per meg' (1 per meg = 10^{-6} = 10^{-3} per mil).

The isotopic fractionation between the parent water and the carbonate precipitated from the water is defined as:

$$^*\alpha_{\text{carbonate/water}} = (\delta^*\text{O}_{\text{carbonate}} + 1000) / (\delta^*\text{O}_{\text{water}} + 1000) \quad (4)$$

where $^*\alpha_{\text{carbonate/water}}$ represents $^{18}\alpha_{\text{carbonate/water}}$ and $^{17}\alpha_{\text{carbonate/water}}$ and the exponent $\theta_{\text{carbonate/water}}$ is defined as:

$$\theta_{\text{carbonate/water}} = \ln(^{17}\alpha_{\text{carbonate/water}}) / \ln(^{18}\alpha_{\text{carbonate/water}}) \quad (5)$$

Reconstructed parent water from speleothem carbonates. Values for $^{18}\alpha_{\text{carbonate/water}}$ and $^{17}\alpha_{\text{carbonate/water}}$ are necessary to back-calculate the triple oxygen isotope composition of the parent waters via a carbonate proxy. Previous studies suggested that different carbonate minerals (e.g., calcite, aragonite), should have very similar $\theta_{\text{carbonate/water}}$ values. Theoretical estimates by Guo and Zhou⁶⁷ for $\theta_{\text{carbonate/water}}$ are 0.525 at 25 °C, and experimental results show values similar to these theoretical predictions: analysis of O_2 derived from the fluorination of modern marine brachiopod shells resulted in values of 0.52486 and 0.52515 at 0 °C and 30 °C, respectively⁶⁸. However, this parameter was predicted to have a potentially minor^{69,70} or moderate⁷¹ temperature sensitivity across

the range of 0–40 °C¹¹, in which the main source of uncertainty for the calculated water triple oxygen isotope compositions is derived from analytical errors, rather than the potential temperature effect on $\theta_{\text{carbonate/water}}$ values. In this study, we calculated the parent water oxygen isotope values using the $\theta_{\text{carbonate/water}}$ value of 0.525 and temperature-specific $^{18}\alpha_{\text{carbonate/water}}$ values⁷². The temperature is based on cave monitoring. The values of the parent water were calculated using a Monte Carlo model combined with statistical estimates of the uncertainty (Supplementary Table 1). Monte Carlo analysis (MC = 1000) was used to reconstruct the isotopic composition of the parent water from speleothem carbonates. The Error calculation includes uncertainties in temperature estimation, speleothem carbonates $\delta^{18}\text{O}$ (0.010‰), and triple oxygen isotope exponent between carbonate and water (0.0001 for $^{18}\alpha_{\text{carbonate/water}}$ and 0.0002 for $\theta_{\text{carbonate/water}}$).

Spatial interpolation. Interpolated maps of the $\delta^{18}\text{O}$ and $\Delta^{17}\text{O}$ values of speleothems were generated using inverse distance weighted (IDW) interpolation⁷³, in ArcGIS 10.1 using the Geostatistical Analyst extension. The spherical semivariogram with a nugget effect was used for the IDW of isotopic data. The quality of the interpolated prediction was tested by cross-validation, which includes prediction at each sample site based on the IDW of the dataset without data from that site.

Moisture sources analysis. Moisture trajectories were derived using the US National Oceanic and Atmospheric Administration (NOAA) HYSPLIT⁷⁴. The moisture source area was determined based on the point density of the trajectories (an hourly point on the trajectory was taken as a point). The moisture back-trajectories are traced back to 120 h for different cave sites for summer (from June to September) and winter (from November to February).

Data availability

The triple oxygen isotope data presented in this paper are available online on the noaa paleoclimate database (<https://www.ncmi.noaa.gov/access/paleo-search/study/38539>). The moisture back-trajectories were computed using the noaa hysplit model based on environmental prediction/national center for atmospheric research, ncep/ncar reanalysis data (https://ready.arl.noaa.gov/hyspxt_traj.php). Reanalyzed precipitation amount and $\delta^{18}\text{O}$ (1980–2015) based on the data from the national centers for environmental prediction/national center for atmospheric research, ncep/ncar (<https://www.esrl.noaa.gov>). The geographic and topographic maps were obtained from global karst aquifer map (wokam project: https://www.un-igrac.org/resource/world_karst-aquifer-map-wokam) and noaa national centers for environmental information (<https://www.ncmi.noaa.gov/products/etopo-global-relief-model>), respectively.

Received: 24 May 2023; Accepted: 4 October 2023;

Published online: 18 October 2023

References

- Gregory, J. M., et al. Climate Change 2021-The Physical Science Basis. *Chem. Int.* <https://doi.org/10.1515/ci-2021-0407> (2021).
- Gimeno, L. et al. The growing importance of oceanic moisture sources for continental precipitation. *Clim. Atmos. Sci.* **3**, 27 (2020).
- Zhang, Q., Sun, P., Singh, V. P. & Chen, X. Spatial-temporal precipitation changes (1956–2000) and their implications for agriculture in China. *Glob. Planet. Change* **82–83**, 86–95 (2012).
- Zhang, Y. T., Hao, Z. C. & Zhang, Y. Agricultural risk assessment of compound dry and hot events in China. *Agric. Water Manag.* **277**, 108128 (2023).
- Luz, B. & Barkan, E. Variations of $^{17}\text{O}/^{16}\text{O}$ and $^{18}\text{O}/^{16}\text{O}$ in meteoric waters. *Geochim. Cosmochim. Acta* **74**, 6276–6286 (2010).
- Li, S. N., Levin, N. E. & Chesson, L. A. Continental scale variation in ^{17}O -excess of meteoric waters in the United States. *Geochim. Cosmochim. Acta* **164**, 110–126 (2015).

7. Li, S. N. et al. Triple oxygen isotope composition of leaf waters in Mpala, central Kenya. *Earth Planet. Sci. Lett.* **468**, 38–50 (2017).
8. Aron, P., et al. Variability and Controls on $\delta^{18}\text{O}$, d-excess, and $\Delta^{17}\text{O}$ in Southern Peruvian Precipitation. *J. Geophys. Res. Atmos.* **126** <https://doi.org/10.1029/2020JD034009> (2021).
9. Tian, C. et al. Spatial and temporal variations of tap water ^{17}O -excess in China. *Geochim. Cosmochim. Acta.* **260**, 1–14 (2019).
10. Surma, J., Assonov, S., Herwartz, D., Voigt, C. & Staubwasser, M. The evolution of ^{17}O -excess in surface water of the arid environment during recharge and evaporation. *Sci. Rep.* **8**, 4972 (2018).
11. Passey, B. H. et al. Triple oxygen isotopes in biogenic and sedimentary carbonates. *Geochim. Cosmochim. Acta.* **141**, 1–25 (2014).
12. Passey, B. H. & Ji, H. Triple oxygen isotope signatures of evaporation in lake waters and carbonates: a case study from the western United States. *Earth Planet. Sci. Lett.* **518**, 1–12 (2019).
13. Huth, T. E. et al. A framework for triple oxygen isotopes in speleothem paleoclimatology. *Geochim. Cosmochim. Acta.* **319**, 191–219 (2022).
14. Sha, L. J. et al. A novel application of triple oxygen isotope ratios of speleothems. *Geochim. Cosmochim. Acta.* **270**, 360–378 (2020).
15. Craig, H. Isotopic variations in meteoric waters. *Science*. **133**, 1702–1703 (1961).
16. Dansgaard, W. Stable isotopes in precipitation. *Tellus*. **16**, 436–468 (1964).
17. Uechi, Y. & Uemura, R. Dominant influence of the humidity in the moisture source region on the ^{17}O -excess in precipitation on a subtropical island. *Earth Planet. Sci. Lett.* **513**, 20–28 (2019).
18. Xia, Z. Y. Quantifying the fingerprint of oceanic moisture source conditions in deuterium and ^{17}O -excess parameters of precipitation. *Geophys. Res. Lett.* **50**, e2022GL101901 (2023).
19. Xia, Z. Y., Surma, J. & Winnick, M. J. The response and sensitivity of deuterium and ^{17}O -excess parameters in precipitation to hydroclimate processes. *Earth-Sci. Rev.* **242**, 104432 (2023).
20. Giménez, R., Bartolomé, M., Gázquez, F., Iglesias, M. & Moreno, A. Underlying climate controls in triple oxygen (^{16}O , ^{17}O , ^{18}O) and hydrogen (^1H , ^2H) isotopes composition of rainfall (Central Pyrenees). *Front. Earth Sci.* **9**, 633698 (2021).
21. Angert, A., Cappa, C. D. & DePaolo, D. J. Kinetic ^{17}O effects in the hydrologic cycle: Indirect evidence and implications. *Geochim. Cosmochim. Acta.* **68**, 3487–3495 (2004).
22. Cheng, H. et al. Milankovitch theory and monsoon. *Innovation* **3**, 100338 (2022).
23. Cheng, H. et al. The Asian monsoon over the past 640,000 years and ice age terminations. *Nature* **534**, 640–646 (2016).
24. Worden, J., Noone, D. & Bowman, K., the Tropospheric Emission Spectrometer science Team and data Contributors. Importance of rain evaporation and continental convection in the tropical water cycle. *Nature* **445**, 528–532 (2007).
25. Lachniet, M. S. Climatic and environmental controls on speleothem oxygen-isotope values. *Quat. Sci. Rev.* **28**, 412–432 (2009).
26. Passey, B. H. & Levin, N. E. Triple oxygen isotopes in meteoric waters, carbonates, and biological apatites: implications for continental paleoclimate reconstruction. *Rev. Mineral. Geochem.* **86**, 429–461 (2021).
27. Zhao, L. J. et al. Factors controlling spatial and seasonal distributions of precipitation $\delta^{18}\text{O}$ in China. *Hydrol. Process.* **26**, 143–152 (2012).
28. Zhang, H. W. et al. Effect of precipitation seasonality on annual oxygen isotopic composition in the area of spring persistent rain in southeastern China and its paleoclimatic implication. *Clim. Past.* **16**, 211–225 (2020).
29. Tian, L. D., et al. Stable isotopic variations in west China: a consideration of moisture sources. *J. Geophys. Res.* **112** <https://doi.org/10.1029/2006JD007718> (2007).
30. Zhou, T. J. & Yu, R. C. Atmospheric water vapor transport associated with typical anomalous summer rainfall patterns in China. *J. Geophys. Res.* **110** <https://doi.org/10.1029/2004JD005413> (2005).
31. Bergel, S. J., Barkan, E., Stein, M. & Affek, H. P. Carbonate ^{17}O -excess as a paleo-hydrology proxy: triple oxygen isotope fractionations between H_2O and biogenic aragonite, derived from freshwater mollusks. *Geochim. Cosmochim. Acta.* **275**, 36–47 (2020).
32. Gázquez, F., Calaforra, J. M., Evans, N. P. & Hodell, D. A. Using stable isotopes ($\delta^{17}\text{O}$, $\delta^{18}\text{O}$ and δD) of gypsum hydration water to ascertain the role of water condensation in the formation of subaerial gypsum speleothems. *Chem. Geol.* **452**, 34–46 (2017).
33. Gázquez, F., et al. The role of cave ventilation in the triple oxygen and hydrogen isotope composition of condensation waters in Altamira Cave, northern Spain. *J. Hydrol.* **606** <https://doi.org/10.1016/j.jhydrol.2021.127416> (2022).
34. Levin, N. E., Raub, T. D., Dauphas, N. & Eiler, J. M. Triple oxygen isotope variations in sedimentary rocks. *Geochim. Cosmochim. Acta.* **139**, 173–189 (2014).
35. Affolter, S. et al. Triple isotope (δD , $\delta^{17}\text{O}$, $\delta^{18}\text{O}$) study on precipitation, drip water and speleothem fluid inclusions for a Western Central European cave (NW Switzerland). *Quat. Sci. Rev.* **127**, 73–89 (2015).
36. Meijer, H. A. J. & Li, W. J. The use of electrolysis for accurate $\delta^{17}\text{O}$ and $\delta^{18}\text{O}$ isotope measurements in water. *Isot. Environ. Health Stud.* **34**, 349–369 (1998).
37. He, S. N., et al. Understanding tropical convection through triple oxygen isotopes of precipitation from the maritime continent. *J. Geophys. Res. Atmos.* **126** <https://doi.org/10.1029/2020JD033418> (2021).
38. Landais, A., Ekaykin, A., Barkan, E., Winkler, R. & Luz, B. Seasonal variations of ^{17}O -excess and d-excess in snow precipitation at Vostok station, East Antarctica. *J. Glaciol.* **58**, 725–733 (2012).
39. Bony, S., Risi, C. & Vimeux, F. Influence of convective processes on the isotopic composition ($\delta^{18}\text{O}$ and δD) of precipitation and water vapor in the tropics: 1. Radiative-convective equilibrium and Tropical Ocean–Global Atmosphere–Coupled Ocean–Atmosphere Response Experiment (TOGA-COARE) simulations. *J. Geophys. Res.* **113** <https://doi.org/10.1029/2008JD009942> (2008).
40. Risi, C., Bony, S. & Vimeux, F. Influence of convective processes on the isotopic composition ($\delta^{18}\text{O}$ and δD) of precipitation and water vapor in the tropics: 2. Physical interpretation of the amount effect. *J. Geophys. Res. Atmos.* **113** <https://doi.org/10.1029/2008JD009943> (2008).
41. Uemura, R., Barkan, E., Abe, O. & Luz, B. Triple isotope composition of oxygen in atmospheric water vapor. *Geophys. Res. Lett.* **37** <https://doi.org/10.1029/2009GL041960> (2010).
42. Galewsky, J. et al. Stable isotopes in atmospheric water vapor and applications to the hydrologic cycle. *Rev. Geophys.* **54**, 809–865 (2016).
43. Xie, C., et al. Precipitation stable isotope composition, moisture sources, and controlling factors in Xi'an, Northwest China. *Atmos. Res.* **280** <https://doi.org/10.1016/j.atmosres.2022.106428> (2022).
44. Surma, J., Assonov, S. & Staubwasser, M. Triple oxygen isotope systematics in the hydrologic cycle. *Rev. Mineral. Geochem.* **86**, 401–428 (2021).
45. Pang, H., Hou, S., Landais, A., Delmotte, V. M. & Jouzel, J. Influence of summer sublimation on δD , $\delta^{18}\text{O}$, and $\delta^{17}\text{O}$ in precipitation, East Antarctica, and implications for climate reconstruction from ice cores. *J. Geophys. Res. Atmos.* **124**, 7339–7358 (2019).
46. Landais, A. et al. Triple isotopic composition of oxygen in surface snow and water vapor at NEEM (Greenland). *Geochim. Cosmochim. Acta.* **77**, 304–316 (2012).
47. Krklec, K. & Dominguez-Villar, D. Quantification of the impact of moisture source regions on the oxygen isotope composition of precipitation over Eagle Cave, central Spain. *Geochim. Cosmochim. Acta.* **134**, 39–54 (2014).
48. Moreno, A. et al. Climate controls on rainfall isotopes and their effects on cave drip water and speleothem growth: the case of Molinos cave (Teruel, NE Spain). *Clim. Dyn.* **43**, 221–241 (2014).
49. Zhou, T. J. et al. Why the western Pacific subtropical high has extended westward since the late 1970s. *J. Climate* **8**, 22 (2009).
50. Huang, R. & Sun, F. Y. Impacts of the Tropical Western Pacific on the East Asian summer. *J. Meteorol. Soc. Jpn.* **70**, 243–256 (1992).
51. Xu, H. et al. Juxta position of western Pacific subtropical high on Asian Summer Monsoon shapes subtropical East Asian precipitation. *Geophys. Res. Lett.* **47**, e2019GL084705 (2020).
52. Ninomiya, K. & Kobayashi, C. Precipitation and moisture balance of the Asian Summer Monsoon in 1991 Part I: precipitation and major circulation systems. *J. Meteorol. Soc. Jpn. Ser. II* **76**, 855–877 (1998).
53. Zhang, J. et al. Seasonal drought events in tropical East Asia over the last 60,000 years. *Proc. Natl. Acad. Sci. USA*. **117**, 30988–30992 (2020).
54. Tao, W., Zheng, L. L., Hao, Y. & Liu, G. P. An extreme gale event in East China under the Arctic potential vorticity anomaly through the Northeast China Cold Vortex. *Adv. Atmos. Sci.* <https://doi.org/10.1007/s00376-023-2255-y> (2023).
55. Chiang, J. C. H., Swenson, L. M. & Kong, W. Role of seasonal transitions and the westerlies in the interannual variability of the East Asian summer monsoon precipitation. *Geophys. Res. Lett.* **44**, 3788–3795 (2017).
56. Molnar, P., Boos, W. R. & Battisti, D. S. Orographic controls on climate and paleoclimate of Asia: thermal and mechanical roles for the Tibetan Plateau. *Annu. Rev. Earth Planet. Sci.* **38**, 77–102 (2010).
57. Coumou, D., Di Capua, G., Vavrus, S., Wang, L. & Wang, S. The influence of Arctic amplification on mid-latitude summer circulation. *Nat. Commun.* **9**, 2959 (2018).
58. Zhang, X. D., Sorteberg, A., Zhang, J., Gerdes, R. & Comiso, J. C. Recent radical shifts of atmospheric circulations and rapid changes in Arctic climate system. *Geophys. Res. Lett.* **35**, L22701 (2008).
59. Sha, L. J. et al. Preparation of high-precision CO_2 with known triple oxygen isotope for oxygen isotope analysis. *Isotopes Environ. Health Stud.* **57**, 443–456 (2021).

60. Paul, D., Skrzypek, G. & Fórizs, I. Normalization of measured stable isotopic compositions to isotope reference scales—a review. *Rapid Commun. Mass Spectrom* **21**, 3006–3014 (2007).
61. Wostbrock, J. A. G. et al. Calibration of carbonate-water triple oxygen isotope fractionation: seeing through diagenesis in ancient carbonates. *Geochim. Cosmochim. Acta* **288**, 369–388 (2020).
62. Coplen, T. B., Kendall, C., & Hopple, J. Comparison of stable isotope reference samples. *Nature* **302**, 236–238 (1983).
63. Duan, P. Z. et al. Comparison of mass spectrometry and spectroscopy methods applied to measurements of water triple oxygen isotopic compositions. *Chi. Sci. Bull.* **66**, 4691–4699 (2021).
64. Schoenemann, S. W., Schauer, A. J. & Steig, E. J. Measurement of SLAP2 and GISP $\delta^{17}\text{O}$ and proposed VSMOW-SLAP normalization for $\delta^{17}\text{O}$ and ^{17}O -excess. *Rapid Commun. Mass Sp.* **27**, 582–590 (2013).
65. Edwards, R. L., Chen, J. H. & Wasserburg, G. J. ^{238}U , ^{234}U , ^{230}Th , ^{232}Th systematics and the precise measurement of time over the past 500,000 years. *Earth Planet. Sci. Lett.* **81**, 175–192 (1987).
66. Cheng, H. et al. Improvements in ^{230}Th dating, ^{230}Th and ^{234}U half-life values, and U–Th isotopic measurements by multi-collector inductively coupled plasma mass spectrometry. *Earth Planet. Sci. Lett.* **371–372**, 82–91 (2013).
67. Guo, W. F. & Zhou, C. Triple oxygen isotope fractionation in the DIC– H_2O – CO_2 system: a numerical framework and its implications. *Geochim. Cosmochim. Acta* **246**, 541–564 (2019).
68. Gibbons, J. A., Sharp, Z. D. & Atudorei, V. Using triple oxygen isotope analyses of biogenic carbonate to reconstruct early triassic ocean oxygen isotopic values and temperatures. *AGU, Fall Meeting*, PP14A-04 <https://api.semanticscholar.org/CorpusID:217158726> (2017).
69. Young, E. D., Galy, A. & Nagahara, H. Kinetic and equilibrium mass-dependent isotope fractionation laws in nature and their geochemical and cosmochemical significance. *Geochim. Cosmochim. Acta* **66**, 1095–1104 (2002).
70. Cao, X. B. & Liu, Y. Equilibrium mass-dependent fractionation relationships for triple oxygen isotopes. *Geochim. Cosmochim. Acta* **75**, 7435–7445 (2011).
71. Pack, A. & Herwartz, D. The triple oxygen isotope composition of the Earth mantle and understanding $\Delta^{17}\text{O}$ variations in terrestrial rocks and minerals. *Earth Planet. Sci. Lett.* **390**, 138–145 (2014).
72. Kim, S. T. & O'Neil, J. R. Equilibrium and nonequilibrium oxygen isotope effects in synthetic carbonates. *Geochim. Cosmochim. Acta* **61**, 3461–3475 (1997).
73. Moyeed, R. A. & Papritz, A. An empirical comparison of kriging methods for nonlinear spatial point prediction. *Math. Geol.* **34**, 365–386 (2002).
74. Draxler, R. R. An overview of the HYSPLIT_4 modelling system for trajectories, dispersion, and deposition. *Aust. Meteorol. Mag.* **47**, 295–308 (1998).
75. Adler, R. F. et al. The Version-2 Global Precipitation Climatology Project (GPCP) monthly precipitation analysis (1979–Present). *J. Hydrometeorol.* **4**, 1147–1167 (2003).
76. Kalnay, E. et al. The NCEP/NCAR 40-Year Reanalysis Project. *Bull. Am. Meteorol. Soc.* **77**, 437–471 (1996).
77. Lu, J. Y. et al. A 120-year seasonally resolved speleothem record of precipitation seasonality from southeastern China. *Quat. Sci. Rev.* **264**, 107023 (2021).
78. Zhang, H. W. et al. Collapse of the Liangzhu and other Neolithic cultures in the lower Yangtze region in response to climate change. *Sci. Adv.* **7**, eabi9275 (2021).
79. Li, T.-Y. et al. Oxygen and carbon isotopic systematics of aragonite speleothems and water in Furong Cave, Chongqing, China. *Geochim. Cosmochim. Acta* **75**, 4140–4156 (2011).
80. Yin, J.-J. et al. Variation in the Asian monsoon intensity and dry-wet conditions since the Little Ice Age in central China revealed by an aragonite stalagmite. *Clim. Past* **10**, 1803–1816 (2014).
81. Zhao, J. Y. et al. Orchestrated decline of Asian summer monsoon and Atlantic meridional overturning circulation in global warming period. *Innovation Geosci.* **1**, 100011 (2023).
82. Zhao, J. Y. et al. Reconstructing the western boundary variability of the Western Pacific Subtropical High over the past 200 years via Chinese cave oxygen isotope records. *Clim. Dynam.* **52**, 3741–3757 (2019).
83. Li, X. et al. The East Asian summer monsoon variability over the last 145 years inferred from the Shihua Cave record, North China. *Sci. Rep.* **7**, 7078 (2017).
84. Li, Y. W. et al. Indian summer monsoon variations during the Younger Dryas as revealed by a laminated stalagmite record from the Tibetan Plateau. *Quat. Sci. Rev.* **278**, 107375 (2022).

Acknowledgements

This work was supported by grants from the National Natural Science Foundation of China (Nos. 41888101, 42103005, 42150710534, 42202218, 42003006, 42272214). Guizhou Provincial Science and Technology Projects (No. [2020]1Y162) to Y.W.L. The Yunnan Fundamental Research Projects (Grant No. 202201AS070022), and the Reserve Talent of the Young and Middle-age Academic and Technical Leader in Yunnan Province (No. 202205AC160025) to T.Y.L. J.A.W. acknowledges support from the Institute for Basic Science (IBS), Republic of Korea, under IBS-R028-Y2. Y.F.N., Y.R.T., and B.Y.Z. are greatly appreciated for their mentoring in all laboratory aspects. We thank X.F. Wang for supporting the speleothem samples from Central Myanmar. We are also grateful for the comments from three anonymous reviewers and editors Dr. Yama Dixit, Dr. Heike Langenberg and Dr. Aliénor Lavergne that helped us significantly improve the manuscript.

Author contributions

H.C. and L.J.S. designed the project. L.J.S. performed the triple oxygen isotope analysis. Y.W.L., J.Y.Z., X.N.Z., P.Z.D., J.W., J.Y.L., H.W.Z., G.K., F.M.B. and T.Y.L. collected the speleothem sample and provided the ^{230}Th dating. L.F.S. and S.L.Z. contributed to the inverse distance weighted (IDW) interpolation. J.Y.R., Q.S.L. and H.Y.L. contributed to the local hydroclimate interpretation. L.J.S. wrote the manuscript with input from H.C., S.M. and J.A.W. All authors contributed to revising the manuscript at various stages.

Competing interests

The authors declare no competing interests.

Additional information

Supplementary information The online version contains supplementary material available at <https://doi.org/10.1038/s43247-023-01043-6>.

Correspondence and requests for materials should be addressed to Lijuan Sha or Hai Cheng.

Peer review information *Communications Earth & Environment* thanks Shyam Ranjan and the other, anonymous, reviewer(s) for their contribution to the peer review of this work. Primary Handling Editors: Yama Dixit, Heike Langenberg and Aliénor Lavergne. A peer review file is available.

Reprints and permission information is available at <http://www.nature.com/reprints>

Publisher's note Springer Nature remains neutral with regard to jurisdictional claims in published maps and institutional affiliations.



Open Access This article is licensed under a Creative Commons Attribution 4.0 International License, which permits use, sharing, adaptation, distribution and reproduction in any medium or format, as long as you give appropriate credit to the original author(s) and the source, provide a link to the Creative Commons license, and indicate if changes were made. The images or other third party material in this article are included in the article's Creative Commons license, unless indicated otherwise in a credit line to the material. If material is not included in the article's Creative Commons license and your intended use is not permitted by statutory regulation or exceeds the permitted use, you will need to obtain permission directly from the copyright holder. To view a copy of this license, visit <http://creativecommons.org/licenses/by/4.0/>.

© The Author(s) 2023